Available online at www.sciencedirect.com
SCIENCE DIRECT®
International Journal of Solids and Structures 43 (2006) 5581–5592
INTERNATIONAL JOURNAL OF SOLIDS and STRUCTURES
www.elsevier.com/locate/ijsolstr

Analysis of localized failure in low-basis-weight paper

R. Hägglund [a], P. Isaksson [b,*]

[a] SCA Packaging Research, Box 716, SE-851 21 Sundsvall, Sweden
[b] Division of Solid Mechanics, Mid Sweden University, SE-851 70 Sundsvall, Sweden

Received 4 May 2005
Available online 17 October 2005

Abstract

Continuum damage mechanics (CDM) is used to describe the post-elastic behavior of low-basis-weight paper. The relevance of undertaking studies of the mechanical behavior of low-basis-weight paper is that it enables characterization, optimization and quality control. In accordance with a CDM theory, an internal variable is introduced that represent the degree to which the material has degraded in a continuum sense and details inherent in a damage evolution law contain information about the rupture mechanism. To account for long ranging micro-structural effects, because of the fiber structure in the paper material, a non-local formulation of the constitutive law is considered. Of particular interest is the fracture toughness of the material, i.e. the ability to resist further crack propagation, as it is often a good measure of flaw tolerance and durability in the context of paper. The constitutive model discussed is verified against tensile tests on rectangular paper specimens containing pre-fabricated cracks. Acoustic emission was used to study the damage evolution in paper specimens during tensile loading. An orthotropic material description has been utilized. The model is contrasted with a purely isotropic formulation. It seems that for the type of problem analyzed in this work, an orthotropic material description does not significantly improve the predictive capability as compared to an isotropic formulation. It is concluded that the model can be used to evaluate the influence of arbitrary defect geometries, defect size and loading conditions and can easily be incorporated into a finite element code.

Keywords: Non-local damage; Fracture mechanics; Low-basis-weight paper; Tensile strength

1. Introduction

Low-basis-weight paper is widely used on a daily basis for a variety of household needs. Several physical properties distinguish them from printing and packaging qualities including tensile response due to a more open network structure offering greater flexibility. Paper essentially consists of a stochastic network of discontinuous cellulose fibers and is usually manufactured by dewatering a cellulose fiber-suspension on a wire. The fibers have an inherent capability to form bonds between them without any additives. Since the fibers are much longer than the thickness of the paper sheet, the network is approximately planar and two-dimensional.

* Corresponding author.
E-mail address: per.isaksson@miun.se (P. Isaksson).

0020-7683/$ - see front matter
doi:10.1016/j.ijsolstr.2005.08.016

In machine-made papers, there are more fibers aligned in the running direction of the paper machine than perpendicular to it. Consequently, at a macroscopic level, paper is often treated as being orthotropic, i.e. having different mechanical properties in three mutually perpendicular planes of symmetry. The principal directions of material symmetry of paper are defined as the machine direction (MD), which is the direction of manufacture, cross direction (CD) and the thickness direction (Z). The relevance of undertaking studies of the mechanical behavior of low-basis-weight paper is that it enables characterization, optimization and quality control. Web breaks is a frequent problem in tissue paper manufacturing. The paper has to be sufficiently strong and the amount defects and variations low in order to endure the converting process, i.e. the process where a hygiene paper product is manufactured by laminating two or several layers of low-basis-weight paper. The process usually includes embossing in order to improve absorbency properties.

In this investigation particular attention is given the tensile response in the cross direction. This is a crucial property because it is generally weaker as compared to the machine direction. Of particular interest is the fracture toughness of the material, i.e. the ability to resist further crack propagation. It is often a good measure of flaw tolerance and durability in the context of paper. The aim of this work is to develop a constitutive model that acknowledges the underlying physics of low-basis-weight paper and is able to quantitatively predict fracture load for paper structures containing defects. In addition, the model should be appropriate to incorporate into a finite element code. Herein, the concept of continuum damage mechanics (CDM) is used to describe the post-elastic behavior. An internal variable is introduced that represent the degree to which the material has degraded in a continuum sense and details inherent in a damage evolution law contain information about the rupture mechanism. The approach is phenomenological, with some attempt to provide a physical interpretation of damage. However, the model is of less use for those whose interest is in seeking the physical mechanisms that cause material deterioration. The model is verified against tensile tests on rectangular paper specimens, tested in CD, containing pre-fabricated cracks manually cut using a razor knife. In addition, acoustic emission monitoring is used to detect the onset and evolution of damage processes obtained in the paper specimens during the tensile tests.

2. Identification of the constitutive behavior

In this section the physical nature of the failure behavior of a wet-creped low-basis-weight paper is discussed. The material has been analyzed in experiments. The mechanical properties depends to great extent on the type and structure of the crepe pattern, which is a wave pattern formed during drying to produce stretchable sheets, Fig. 1. The material is made from chemical pulp having a basis weight of 23 g/m^2. The material consists of fibers having a length-weighted-average fiber length of 2.2 mm and an average fiber width of 23 μm. The experiments were conducted in a 23 °C and 50% RH climate, which in accordance with ISO 187. The samples were conditioned for more than 48 h in this climate prior to testing.

2.1. Tensile test

The material was investigated by means of load–elongation curves in both CD and MD. The tensile tests were conducted in a MTS universal testing machine. Specimens were tested at a deformation rate of 1.2 mm/min. In order to monitor the damage behavior during the process of loading, an acoustic emission (AE) sensor

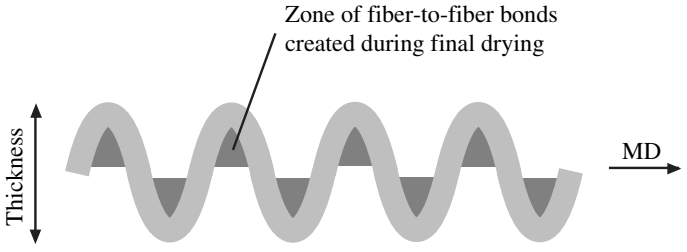

Fig. 1. Sketch of a crepe pattern.

was mounted in the center of the specimen. Acoustic emission is a well-established technique for analysis of damage evolution in paper and the interested reader is advised to, among others, (Gradin et al., 1997; Yamauchi, 2004; or Isaksson et al., in press). The basic principle in AE is that during the fracturing of a fiber or a fiber-to-fiber bond (which will occur in the order of micro seconds), stresses in the neighborhood of the fracture site will be redistributed and cause a rapid release of elastic energy. This redistribution will in general be transmitted through the material as an elastic wave, which can be recorded on the surface of the material, using an appropriate acoustic emission sensor. In this way each fracturing of a fiber or a fiber-to-fiber bond is the source of one acoustic emission event. The sensor, manufactured by the Acoustic Emission Technology Company (AET), had a resonance frequency of 300 kHz. A computer system from Vallen Systeme GmbH was used to record and store the AE-signals. A typical result is displayed in Fig. 2, which shows both the load–displacement curves as well as the cumulative number of acoustic events from experiments performed in CD and MD.

It is observed in Fig. 2 that the stress–strain response exhibits a pronounced non-linear behavior in both MD and CD prior to rupture, which is in agreement with previous studies on low-basis-weight paper (cf. Hollmark, 1983; or Ramasubramanian, 2002). The crepe structure is reflected in the results in that the strain at peak is higher in MD as compared to CD. The higher peak-load (tensile strength) in MD is a consequence of the fiber alignment. It was observed that damage localized to narrow bands at ultimate load. In CD, the AE response is approximately exponential. However, in MD the AE response is initially linear and switches eventually to an exponential response prior to ultimate load. The linear part is believed to reflect the straightening and removal of the crepe structure. In the wet crepeing process, some bonds are established between fibers in the creped sheet during the final drying, i.e. after formation of the wave shape (Hollmark, 1983), illustrated in Fig. 1. These bonds break continuously from the early stage of loading. It is here believed that it is breakage of this type of bonds that cause the initial linear response in the AE characteristics. At high loads the crepe structure disappears as the structure is stretched and the specimen seems to rupture in approximately the same manner as the specimens does in CD. Due to the low stiffness, the material exhibit a stable, or semi-stable, failure behavior at post-peak elongations even for a gauge length of 100 mm. This is due to that a relatively small amount of strain energy is stored in the specimen prior to rupture.

2.2. Failure analysis using SEM

Damage features of the considered material were examined using an extended pressure scanning electron microscope (SEM). The system is equipped with a miniature tensile testing device with a 300 N load cell. Specimens with opposite semi-circular edge notches were used in order to steer the site of failure localization, Fig. 3. The gauge length was 10 mm and the specimen was loaded at a deformation rate of 0.1 mm/min. The high stress region at the edge of the notch was monitored during the process of loading.

Figs. 4 and 5 shows micrographs of progressive damage in the vicinity of the notch for specimens loaded in CD and MD. The pictures correspond to consecutive load levels at the time of formation of a macroscopic crack. The crack's initiation site is an important step in determining the root cause of failure. In paper of this

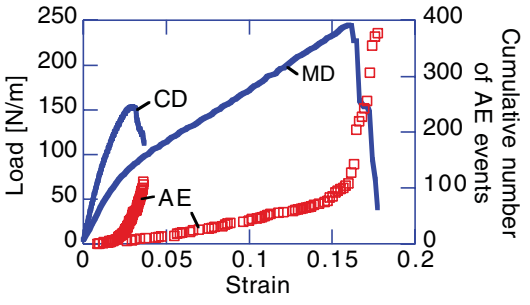

Fig. 2. Typical force–displacement curves in CD and MD and cumulative number of AE events. The width of the specimens was 50 mm and the gauge length 100 mm.

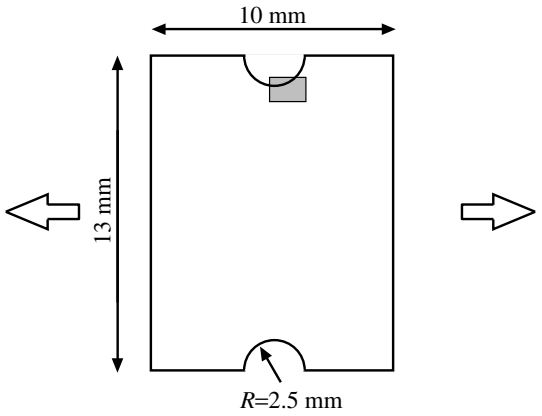

Fig. 3. Specimens with opposite semi-circular edge notches.

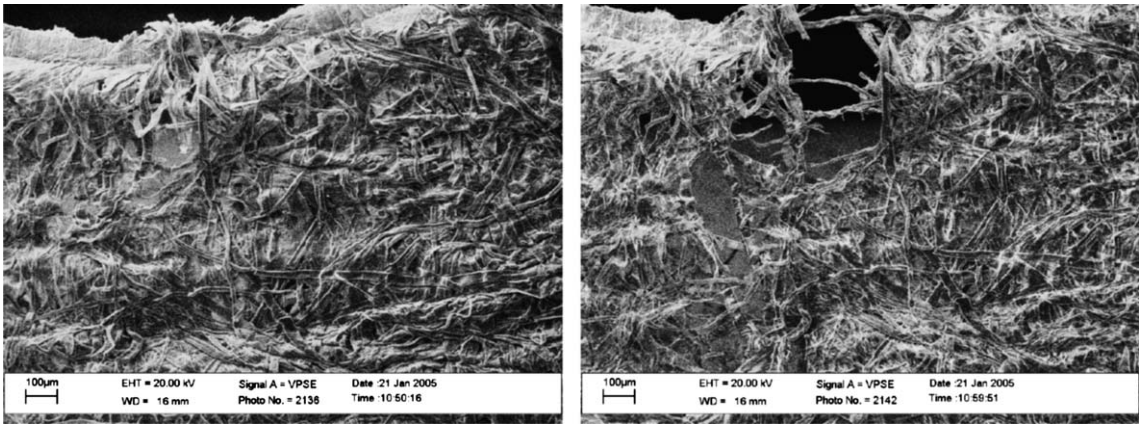

Fig. 4. SEM micrograph of the damage zone during tensile loading in CD.

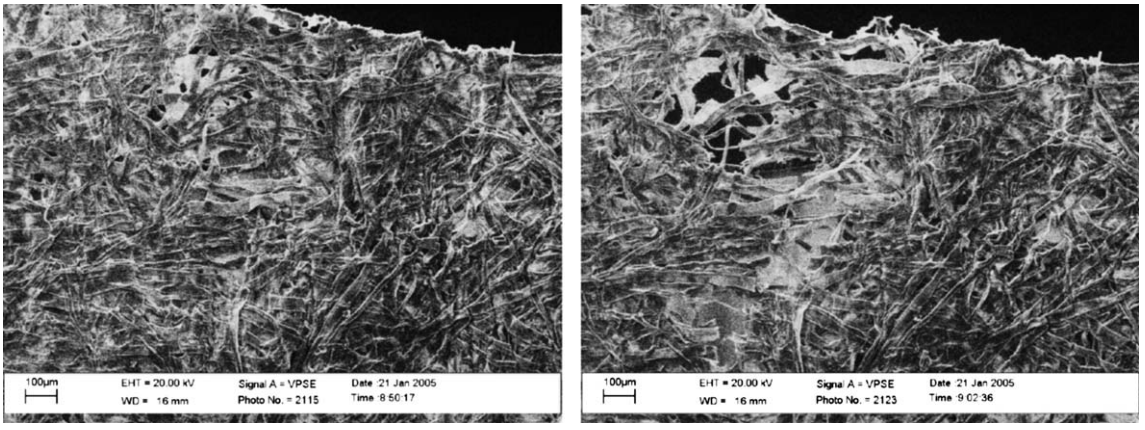

Fig. 5. SEM micrograph of the damage zone during tensile loading in MD.

type there exist significant variations in the structural properties, which is a result of the manufacturing process. According to the micrographs, failure seems to localize to initially sparse regions of the network. The inherent variations in the material seem to govern the exact location of the formation of a macroscopic crack.

In Fig. 4 (CD), the crepe pattern is observed as wrinkles oriented in the loading direction. In Fig. 5 (MD), the crepe wrinkles are no longer visible at the time of failure since the structure has been stretched. The damage process seems to be dominated by progressive debonding; fibers are pulled out from the network. However, a few fiber breaks can be observed in the damage zones.

2.3. Constitutive behavior

The objective is to derive a constitutive model that captures the over-all mechanical behavior of the material and the ambition is to keep the number of model parameters at a minimum. The principles and terminology of CDM is employed. A key feature of the tensile response of the considered material is the large amount of damage due to bond breaks observed in experiments. This progressive physical process of degradation of the mechanical properties up to complete failure is commonly referred to as damage. Herein, a clear distinction is made between "damage" and "plasticity". In the context of paper it is convenient to define a damage process as the irreversible process where either a fiber or a fiber-to-fiber bond breaks, while a plastic process is when there is an irreversible straining of the fibers themselves. For low-basis-weight paper it is reasonable to assume that there is no significant amount of plastic deformation of the fibers, which is motivated by the open network structure leading to a low degree of bonding and consequently low axial stress in the fibers prior to failure. Fiber breakage is the critical factor for paper strength only if the bonds are very strong or the fibers weak. Based on the results from the experiments and previous investigations it is believed that the tensile response of the considered material is essentially an example of brittle damage, i.e. damage without accompanying plasticity (cf. Krajcinovic and Foneska, 1981; or Krajcinovic, 1983, 1996). In the tensile test it was observed that damage localizes in bands during the final stage of failure. Localization of damage in sparse networks has been analyzed using network models (cf. Heyden and Gustafsson, 1998; Åström and Niskanen, 1993; or Ritala and Huiku, 1989). However, the exact mechanisms for localization of damage in paper materials have not been fully established. Experimentally it has been shown, for dense paper structures, that the width of the damage zone in paper is governed by the fiber length (Niskanen et al., 2001). The behavior can be explained by that all fibers are coupled to a number of other fibers, each fiber apply non-local actions within a limited volume. In this study, to account for such long ranging micro-structural effects, a non-local formulation of the constitutive equation is used. Generally, non-local formulations are accomplished by spatial averaging of some quantity. An intrinsic material length scale parameter is incorporated into the constitutive description. There exist different techniques to incorporate non-locality. Examples of such formulations include non-local integral formulations (cf. Kröner, 1967; or Eringen and Edelen, 1972) and gradient theories (cf. Geers, 1997; or de Borst et al., 1999). In this paper a gradient approach is utilized. Recently, it has been shown (Isaksson et al., in press) that the presence of stress gradients has a large influence on the mechanisms that control the damage processes in paper materials. It was demonstrated, in a combined experimental and numerical study, that when stress gradients are present in a paper material, a non-local theory has to be introduced in the analysis to properly describe onset and progression of damage on the continuum level. According to the theory: the larger a gradient sensitivity length is, the higher local stresses and strains can the material tolerate without suffering any material degradation as long as stress gradients are present. In contrast to local theory, the non-local model is capable of capturing strain-softening and localization behavior. Non-local models have been reviewed by, e.g. Jirásek (1998), to whom the interested reader is advised.

3. Formulation of the constitutive model

The mathematical formulation of a model for damage coupled to elastic deformation is presented. The model discussed herein is very much influenced by the work of e.g. Peerlings et al. (1996) or Pijaudier-Cabot and Bazant (1987). Damage is realized by introducing an isotropic scalar damage parameter D characterizing the degradation of the material. Virgin material is characterized by $D = 0$ while $D = 1$ corresponds to a fully ruptured element. The assumption of one single isotropic damage variable is justified because of the nature of the prevailing damage mechanism, i.e. fiber-to-fiber bond breaks. If the bond is loaded in the plane of the sheet, it is believed that the strength of such bond is independent of in which direction it is loaded. In contrast to this, it has been shown that anisotropic dense paper structures where fiber breaks is the dominating damage

mechanism, requires one damage parameter for each in-plane direction to describe the damage behavior properly (cf. Isaksson et al., 2004). This may be explained by that the fiber breakage is a directional dependent failure mechanism because the fracture plane is perpendicular to the direction of the fiber.

An assumption of the elastic energy equivalence principle is made (cf. Cordebois and Sidoroff, 1982; or Hansen and Schreyer, 1994) which means that the elastic energy density in a material element of a damaged material is of the same form as that of an undamaged material except that the stress tensor σ_{ij} is replaced by an effective stress tensor $\hat{\sigma}_{ij}$ according to

$$\sigma_{ij} = (1 - D)\hat{\sigma}_{ij}. \tag{1}$$

Obviously, $\sigma_{ij} = \hat{\sigma}_{ij}$ for an undamaged material and $\sigma_{ij} \to 0$ at the moment of rupture. Using (1), the expression for the stress increment $\mathrm{d}\sigma_{ij}$ in the damage stress space is obtained as $\mathrm{d}\sigma_{ij} = (1 - D)\mathrm{d}\hat{\sigma}_{ij} - \hat{\sigma}_{ij}\mathrm{d}D$. If it is assumed that one scalar parameter D describes damage in a point, then the driving force for damage evolution in that point is given by the local damage energy release rate Y defined as $Y = \mathrm{d}\psi/\mathrm{d}D$, where ψ is the elastic stress energy (complementary energy), given by (cf. Hansen and Schreyer, 1994)

$$\psi = \frac{1}{2}\hat{\sigma}_{ij}C^{-1}_{ijkl}\hat{\sigma}_{kl}. \tag{2}$$

Here, C_{ijkl} is the stiffness tensor. Thus, according to the postulate of elastic energy equivalence, one obtains with use of (1)

$$Y = (1 - D)^{-3}\sigma_{ij}C^{-1}_{ijkl}\sigma_{kl}. \tag{3}$$

For a local damage theory, this means that when Y reaches a critical value Y_0 in a certain point, damage will start in that point. However, due to the non-local nature of paper, a non-local damage driving force $\bar{Y}$ is introduced. The technique was originally developed by Pijaudier-Cabot and Bazant (1987) and the concept has successfully been applied to analyze tensile response of different types of paper materials (Isaksson et al., 2004, in press). A numerically efficient technique based gradient theory is used which includes incorporation of an additional partial differential equation according to

$$\overline{Y} = Y + c^2\nabla^2 Y, \tag{4}$$

where c is a gradient length parameter (cf. Lasry and Belytschko, 1988; or Mühlhaus and Aifantis, 1991). The Laplacian operator is defined as $\nabla^2 = \sum_i \partial^2/\partial x_i^2$. Among others, Peerlings et al. (1996) and later Geers (1997) approximated equations of the class of the explicit formulation in (4) with an implicit gradient enhanced formulation resulting in an inhomogeneous elliptic equation that is suitable to incorporate in finite element analyses:

$$\bar{Y} - \frac{1}{2}l^2\nabla^2\bar{Y} = Y, \tag{5}$$

where derivatives of order four and higher have been neglected. It is here assumed that $\bar{Y}$ admit at least Fréchet derivative. The gradient sensitivity parameter l in (5) is a characteristic length that controls the range of non-local actions and must therefore be related to the scale of the microstructure in the material. Moreover, the solution of (5) requires additional boundary conditions. Following Lasry and Belytschko (1988) or Mühlhaus and Aifantis (1991) the natural Neumann type boundary condition of a vanishing gradient is used along the boundary Γ surrounding the entire problem domain,

$$n\nabla\bar{Y} = 0, \tag{6}$$

where n is the outward normal to the boundary Γ. It should be underlined that a physical interpretation of this boundary condition is not clear.

The details inherent in the damage evolution law contain the information about the rupture mechanism. An irreversible damage evolution law is formulated as

$$\mathrm{d}D = k(1 - D)\,\mathrm{d}\bar{Y} \quad \text{for } \bar{Y} = R, \tag{7}$$

where k is a material parameter commonly referred to as damage hardening. The threshold R is interpreted as the maximum value that $\bar{Y}$ has reached during the deformation history (with the initial value Y_0) thus representing an isotropic damage hardening material. It has been shown that the damage evolution law (7) describes the degradation in different types of paper materials reasonably well (Isaksson et al., 2004, in press) in situations of continuous loading.

4. Verification for mode I tensile fracture

In this section the constitutive model described in Section 3 is evaluated. A tensile loaded rectangular specimen consisting of low-basis-weight paper containing a pre-fabricated slit is examined. The analysis corresponds to a rectangular central cracked specimen during tensile mode I loading (i.e. opening mode). Such analysis enables evaluation of the non-local feature of the constitutive model because damage is localized to the tip of the notch. The effect of a notch size is investigated. Fracture of notched bodies has been studied using CDM in several investigations (among others: Geers, 1997; de Borst et al., 1999; Dhar et al., 2000; or Ferrara and di Prisco, 2001). The geometry of the specimen is visualized in Fig. 6. The dimension of the specimen is given by the size of the crack ($2a$), gauge length ($2h$) and the width of the specimen ($2w$). A quarter region is analyzed owing to the symmetry of the boundary conditions and loading. The predicted fracture loads are obtained when the overall damage of a material point reaches the critical value 1 as it is here assumed that onset of macroscopic crack growth occur when $D \to 1$.

4.1. Numerical implementation and boundary conditions

The boundary conditions of the reduced geometry shown in Fig. 6 is given by

$$\begin{aligned} &\sigma_x = 0 \quad \text{for } x = w \\ &u_y = 0 \quad \text{for } a < |x| \leqslant w \quad \text{and} \quad y = 0 \\ &\tau_{xy} = \sigma_y = 0 \quad \text{for } 0 < |x| \leqslant a \quad \text{and} \quad y = 0 \\ &u_x = 0 \quad \text{for } x = 0 \\ &u_y = u_0 \quad \text{for } x = h \end{aligned} \tag{8}$$

The displacements in the x- and y-directions are denoted u_x and u_y, respectively, according to the Cartesian coordinate system in Fig. 6. σ_x and σ_y are the normal stresses and τ_{xy} is the shear stress. Additionally, the natural boundary condition of a vanishing gradient of the non-local damage energy release rate on the boundaries is used, i.e. (6). The problem has been analyzed using the finite element method. The finite element procedure follows mainly the ones discussed in Peerlings et al. (1996) and Geers (1997) for an enhanced gradient model. Four-node isoparametric elements with two degrees of freedom, translation in the x- and y-directions, have been utilized. The entire mesh consists of approximately 800 elements. An iterative technique has been

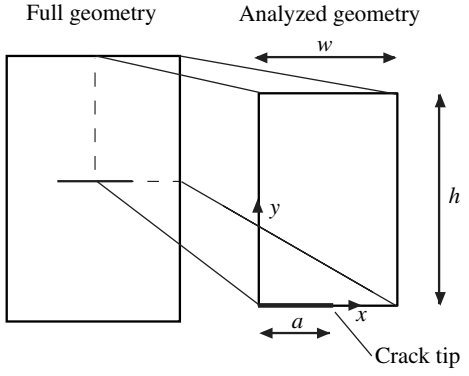

Fig. 6. Center cracked specimen.

employed to solve the equilibrium equations at each load step. The result obtained after each iteration then corresponds to estimates of the incremental displacements from which the current stress and damage states are computed. The numerical scheme was implemented in the Matlab (2002) code, which offers a language for numerical computing. All deformations are assumed to be small so that linear relations for equilibrium and kinematics are applicable and all derivatives and integrals are evaluated with respect to the initial topology of the considered body. The non-local formulation of the constitutive law guarantees that no spurious effects arise in the numerical solution.

4.2. Experiments on rectangular specimens containing a pre-fabricated slit

Tensile tests on rectangular specimens containing pre-fabricated slits (notches) were conducted. An important issue in the present verification is the reliable prediction of size and notch effects. Load–elongation response was measured using specimens having a width and gauge length of 150 mm ($2w$) and 230 mm ($2h$), respectively, at a deformation rate of 1.6 mm/min. The specimens were tested in CD only. The pre-fabricated crack was manually cut in the center of the specimen oriented in MD to a length ($2a$) ranging from 5 to 70 mm.

4.3. Calibration of the constitutive model

The constitutive model was calibrated using data from tensile tests similar to the ones presented in Fig. 2. To obtain an approximately uniaxial and homogenous stress field, the size of the specimens were 100×30 mm. Because use is made of an orthotropic material description to describe the elastic response of the considered material, the model parameters are estimated from tensile tests in both CD and MD. The model requires five elastic parameters ($E_1, E_2, G_{12}, \nu_{12}, \nu_{21}$) that describes the elastic behavior, two parameters (Y_0, k) that characterizes the (isotropic) damage evolution and a gradient parameter (l) that controls the range of non-local mechanisms. Here the index 1 refers to CD and index 2 to MD. The elastic modulus in CD and MD of the material were determined from the initial slope of the load–displacement curves and were estimated to be $E_1 = 6.3$ kN/m and $E_2 = \frac{1}{2}E_1$ (compare to Fig. 2). The in-plane Poisson's ratios could not be obtained in experiments but were set to $\nu_{12} = 0.45$ and $\nu_{21} = 0.22$. The in-plane shear modulus was assigned the value $G_{12} = 0.4\sqrt{E_1 E_2}$ following Baum et al. (1981). The damage hardening parameter (k) was determined by fitting the constitutive model to the post-elastic regime of the load–displacement curve when loaded in CD. Displayed in Fig. 7 are four experimentally obtained load–displacement curves. The damage threshold (Y_0) was obtained from onset of AE. The calibration procedure gave values of $Y_0/E_1 = 6.5 \times 10^{-5}$ and $kY_0 = 7.5 \times 10^{-3}$. The straight dotted line in Fig. 7 indicates the linear force–displacement response one would have if the material remained undamaged.

4.4. Results: comparison between model and experiment

Fig. 8 shows a comparison of the damage behavior between the model (FEM) and an AE experiment for the 100×30 mm specimens tested in CD. The actual force–displacement experiment at which the acoustic

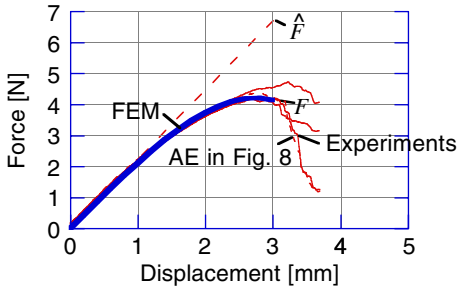

Fig. 7. Calibration of damage parameters. Specimens are loaded in CD.

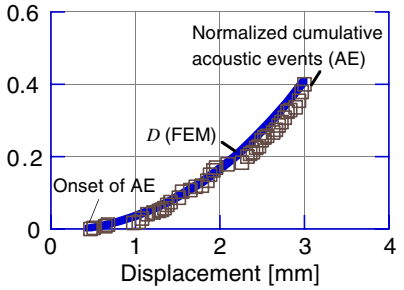

Fig. 8. Damage evolution during tensile loading. Both computed damage (FEM) and measured damage (AE) is displayed.

activity was monitored is indicated in Fig. 7. The comparison is based on the assumption that D is homogenous in the material and proportional to the cumulative number of acoustic events. The comparison is made in the displacement interval 0–3 mm. For displacements larger than 3 mm, the specimen ruptured in an unstable manner as localization took place and eventually a final crack was formed. Obviously, when localization is reached the damage growth is not homogenous and the measured AE is difficult to interpret.

With reference to Fig. 7, at the displacement 3 mm the experimentally obtained load is $F \approx 4.1$ N and the estimated corresponding load of an undamaged specimen is $\hat{F} \approx 6.7$ N. Assuming the damage in the specimen is isotropic and homogenous and by using (1) one may estimate the level of damage in the specimen as $D^* = 1 - F/\hat{F} \approx 0.4$ at the displacement 3 mm. Then, by using the estimated degree of damage, the cumulative number of AE events was normalized so that the total number of cumulative events at the displacement 3 mm corresponds to a damage level of $D^* = 0.4$ in the material. As shown in Fig. 8, the agreement between the measured and computed damage is satisfying.

The intrinsic length parameter l cannot be determined from testing of rectangular specimens since they produce an almost homogenous stress field during conventional tensile testing and the influence from the stress gradients vanishes. Fig. 9 shows a comparison between the model and experiments for notched specimens. The 95% confidence limit is presented along with the average value of eight specimens for each notch length. The computed results of fracture load (i.e. peak-load) are presented for three different values of l. In Fig. 9, the length of the slit has been normalized with respect to the width of the specimen and fracture load against the tensile strength of the material (i.e. the peak-load of an un-notched specimen). Obviously, as the stress field is approximately homogenous for an un-notched specimen, the influence of l vanishes and $\bar{Y}/Y \to 1$ as $a/w \to 0$. According to the results, slits smaller than 10–15 mm has marginal influence on the fracture load. For short crack lengths (<10 mm) the pre-fabricated crack frequently failed to localize failure in experiments as formation of a macroscopic crack took place outside the plane of the main crack. Thus, for the case of small defects failure may localize to inherent weak spots in the sheet. According to the results presented in Fig. 9 there seems to be a good agreement between the model and experiments for $l \approx 5$ mm, which is roughly twice the size of the length-averaged fiber length. This is in agreement with previous investigations on packaging paper where it has been concluded that the intrinsic length was approximately twice the length-averaged fiber

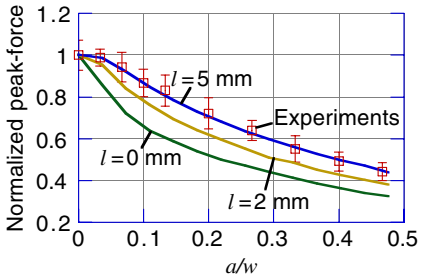

Fig. 9. Comparison between the model (FEM) and experiments performed in CD. The peak-force is normalized with the tensile strength of the material.

length (Isaksson et al., 2004). Whether there is a relation between the two quantities should be investigated in a forthcoming study where the coupling between the fiber length and the intrinsic length parameter in the non-local model should be evaluated.

The material develops a relatively large damage zone in the vicinity of the crack tip prior to rupture and thereby falling out of the scope of linear elastic fracture mechanics (LEFM) for most applications. Fig. 10 shows contour plots of the computed damage parameter in the vicinity of the crack tip for $2a = 50$ mm and $l = 5$ mm at onset of crack growth, i.e. $\max\{D\} \to 1$. For the sake of illustration, a contour plot is also displayed for the situation of an isotropic material description (elastic modulus $E = E_1$ and Poisson's ratio $v = 0.3$). According to the model, the process zone extends approximately 30 mm from the crack-tip. There is a striking similarity between the results obtained from the orthotropic and isotropic material descriptions. For the sake of comparison, the contour plot obtained with use of an isotropic material description (Fig. 10b) is accompanied with an estimate of a diffuse damage zone obtained using a second order Irwin approximation (cf. Anderson, 1991; or Bazant and Planas, 1998), which is considered to be a rough estimate of the process zone. The approximation of the extension r_p of a damage zone ahead of the crack tip is given by the tensile strength σ_0 and the critical mode I stress intensity factor K_{Ic} according to $r_p = K_{Ic}^2/[\pi\sigma_0^2]$. Here, K_{Ic} is obtained by using the LEFM relation $K_{Ic} = 1.12\sigma_c(\pi a)^{1/2}$ (cf. Anderson, 1991) where σ_c is the fracture stress. Using

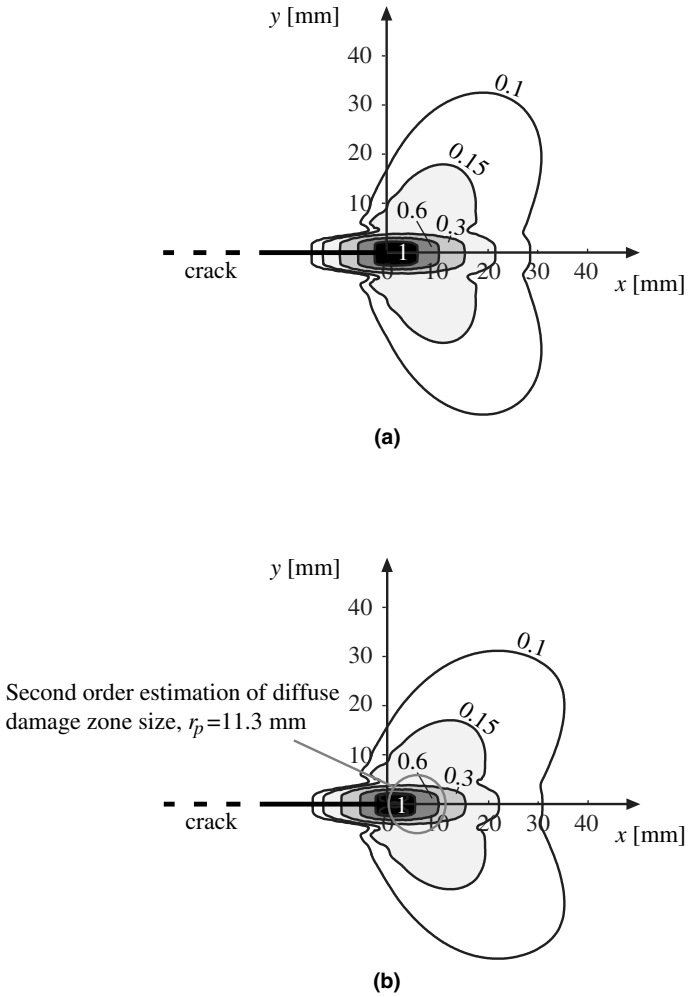

Fig. 10. Contour plots of the damage variable D in the vicinity of the crack-tip located at $x = 0$ and $y = 0$: (a) orthotropic and (b) isotropic material description.

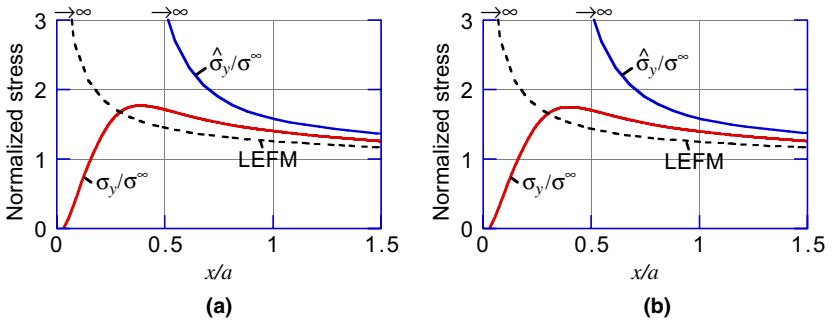

Fig. 11. Normalized stresses in-front of the crack-tip along the plane of a crack, $x > 0$ and $y = 0$: (a) orthotropic and (b) isotropic material description. The remote stress σ^{∞} is acting at the boundaries $|y| = h$.

Fig. 9, the ratio $\sigma_c/\sigma_0 \approx 0.6$ is readily obtained for the crack length ratio $a/w = 1/3$. The estimation gives a non-linear zone of size $r_p \approx 11.3$ mm.

The corresponding normal stresses in the y-direction are presented in Fig. 11 for the same cases as in Fig. 10. Of significant interest is the distribution of the effective stress $\hat{\sigma}_y$ since the effective stresses are referred to a surface in the material that really transmits the internal forces (see amid others Simo and Yu, 1987; or Lemaitre and Chaboche, 1990). The stresses in Fig. 11 are normalized with the remote normal stress σ^{∞} acting at the boundaries $|y| = h$ at crack growth. For the sake of illustration, the corresponding normalized normal stress according to LEFM is also displayed for the case of an un-damaged material and the same peak-force. An important conclusion of the results shown in Fig. 11 is that the incorporation of an orthotropic material description does not significantly improve the predictive capability of the model. This behavior is a result of the non-local formulation as the damage processes are significantly influenced by the stress field far away from the near-tip region, which is approximately uniaxial.

Noteworthy in Fig. 11 is that—at crack growth—the effective stress $\hat{\sigma}_y$ in the crack-tip region tends to infinity on a greater distance relative the crack-tip than the "classical" normal stress according to LEFM. This is a result of the non-local formulation, which smears stresses over a domain having a size governed by the intrinsic length l, i.e. (5). The results presented in Figs. 9 and 11 both indicates that the considered paper material seems to tolerate much higher stresses than what is expected according to the classical theories of local actions and LEFM, hence confirms the discussion made in Sections 2 and 3.

5. Conclusions

Localized damage and fracture in creped low-basis-weight paper has been examined. The material is made from chemical pulp having a basis weight of 23 g/m^2. A non-local constitutive model was developed following a theory of continuum damage mechanics. The model was compared to the experimentally obtained tensile fracture behavior of notched paper specimens in the cross-direction (CD) for a wide range of notch sizes. On the basis of this investigation, the model has the potential to describe the tensile fracture response of low-basis-weight paper. Although the resulting mathematical structure is not simple, we believe that this is the simplest constitutive equation that is consistent with the basic requirements of continuum mechanics and the physics of damage in low-basis-weight papers. It was found that the length parameter controlling the range of non-local actions generated results that agreed with experiments for a value of 5 mm, which is approximately twice the size of the length-averaged fiber length in the material. This observation is in agreement with previous observations on paper materials where non-local models has been used and may support the assumption that fiber length controls the range of non-local actions in the considered material. Further on, acoustic emission monitoring of the damage processes supports the use of an exponential damage evolution law for tissue base paper in CD. It is believed that the model can be used to evaluate the influence of arbitrary defect geometries, defect size and loading conditions and can easily be incorporated into a finite element code. Finally, orthotropic and isotropic material descriptions seems to generate similar results for the case studied in

this work. Hence, for low-basis-weight paper, an isotropic material description may be sufficient if the stress field outside the immediate vicinity of a defect site (i.e. crack) is approximately uniaxial.

References

Anderson, T.L., 1991. Fracture Mechanics: Fundamentals and Applications. CRC Press, Boca Raton, USA.

Baum, G.A., Brennan, D.C., Habeger, C.C., 1981. Orthotropic elastic constants of paper. Tappi 64, 97–101.

Bazant, Z., Planas, J., 1998. Fracture and Size Effect in Concrete and Other Quasibrittle Materials. CRC Press, Boca Raton, USA.

Cordebois, J.P., Sidoroff, F., 1982. Damage induced elastic anisotropy. In: Boehler, J.P. (Ed.), Mechanical Behaviour of Anisotropic Materials. CNRS, Paris, France.

de Borst, R., Pamin, J., Geers, M.G.D., 1999. On coupled gradient-dependent plasticity and damage theories with a view to localization analysis. Eur. J. Mech. A/Solids 18, 939–962.

Dhar, S., Dixit, P.M., Sethuraman, R., 2000. A continuum damage mechanics model for ductile fracture. Int. J. Pres. Ves. Pip. 77, 335–344.

Eringen, A.C., Edelen, D.G.B., 1972. On nonlocal elasticity. Int. J. Eng. Sci. 10, 233–248.

Ferrara, L., di Prisco, M., 2001. Mode I fracture behavior in concrete: non-local damage modelling. ASCE J. Eng. Mech. 127, 678–692.

Geers, M.G.D., 1997. Experimental analysis and computational modelling of damage and fracture. Ph.D. Thesis. Eindhoven University of Technology, The Netherlands.

Gradin, P., Nyström, S., Flink, P., Forsberg, S., Stollmaier, F., 1997. Acoustic emission monitoring of lightweight coated paper. J. Pulp Paper Sci. 23, 113–118.

Hansen, N.R., Schreyer, H.L., 1994. A thermodynamically consistent framework for theories of elastoplasticity coupled with damage. Int. J. Solids Struct. 31, 359–389.

Heyden, S., Gustafsson, P.J., 1998. Simulation of fracture in a cellulose fibre network. J. Pulp Paper Sci. 24, 160–165.

Hollmark, H., 1983. Mechanical properties of tissue. In: Mark, R.E. (Ed.), Handbook of Mechanical Testing of Paper and Paperboard. Marcel Dekker, New York, USA.

Isaksson, P., Hägglund, R., Gradin, P., 2004. Continuum damage mechanics applied to paper. Int. J. Solids Struct. 41, 4731–4755.

Isaksson, P., Gradin, P.A., Kulachenko, A., in press. The onset and progression of damage in isotropic paper sheets. Int. J. Solids Struct., doi:10.1016/j.ijsolstr.2005.04.035.

Jirásek, M., 1998. Nonlocal models for damage and fracture: comparison of approaches. Int. J. Solids Struct. 35, 4133–4145.

Kröner, E., 1967. Elasticity theory of materials with long range cohesive forces. Int. J. Solids Struct. 3, 731–742.

Krajcinovic, D., 1983. Constitutive equations for damaging materials. J. Appl. Mech. 50, 355–360.

Krajcinovic, D., 1996. Damage Mechanics. Elsevier, Amsterdam, The Netherlands.

Krajcinovic, D., Foneska, G.U., 1981. The continuum damage theory of brittle materials. J. Appl. Mech. 48, 809–824.

Lasry, D., Belytschko, T., 1988. Localization limiters in transient problems. Int. J. Solids Struct. 24, 581–597.

Lemaitre, J., Chaboche, J.L., 1990. Mechanics of Solid Materials. Cambridge University Press, Cambridge, UK.

Matlab, 2002. Version 6.5. The MathWorks Inc., Natick, MA USA.

Mühlhaus, H.-B., Aifantis, E.C., 1991. A variational principle for gradient plasticity. Int. J. Solids Struct. 28, 845–857.

Niskanen, K., Kettunen, H., Yu, Y., 2001. Damage width: a measure of the size of fracture process zone. In: 12th Fundamental Research Symposium, Oxford, UK.

Pijaudier-Cabot, G., Bazant, Z.P., 1987. Nonlocal damage theory. J. Eng. Mech. 113, 1512–1533.

Peerlings, R.H.J., de Borst, R., Brekelmans, W.A.M., de Vree, J.H.P., 1996. Gradient enhanced damage for quasi-brittle materials. Int. J. Numer. Methods Eng. 39, 3391–3403.

Ramasubramanian, M.K., 2002. Mechanical properties and testing of towel and tissue papers. In: Mark, R.E. (Ed.), Handbook of Physical and Mechanical Testing of Paper and Paperboard. Marcel Dekker, New York, USA.

Ritala, R.K., Huiku, M.T., 1989. Scaling, percolation and network theories: new insight into papermaking. In: Trans. 9th Fundamental Research Symposium, Cambridge, UK, pp. 195–218.

Simo, J.C., Yu, W., 1987. Strain and stress-based continuum damage models—I. Formulation. Int. J. Solids Struct. 23, 821–840.

Yamauchi, T., 2004. Effect of notches on micro failures during tensile straining of paper. Jpn. Tappi J. 58, 105–112.

Åström, J., Niskanen, K., 1993. Symmetry-breaking fracture in random fibre networks. Europhys. Lett. 21, 557–562.